Polymer Journal (2011) 43, 370–377

www.nature.com/pj

ORIGINAL ARTICLE

Significant increase in the melting temperature of poly(ε-caprolactone) blocks confined in the crystallized lamellar morphology of poly (ε-caprolactone)-*block*-polyethylene copolymers

Takuya Sakurai and Shuichi Nojima

The melting temperature of poly(ε-caprolactone) (PCL) blocks, $T_{m,PCL}$, in PCL-*block*-polyethylene (PCL-*b*-PE) is investigated as a function of the volume fraction of PCL blocks in the system, ϕ_{PCL}, and compared with that in PCL-*block*-polybutadiene (PCL-*b*-PB), the precursor of PCL-*b*-PE with an identical PCL molecular weight. The amorphous PCL block in PCL-*b*-PE is spatially confined within the solid lamellar morphology formed by the advance crystallization of PE blocks (PE lamellar morphology), which will bring about a considerable depression in the conformational entropy of amorphous PCL blocks. On the other hand, PCL-*b*-PB forms some microdomain structure when the PCL block is amorphous, so that the conformational entropy of amorphous PCL blocks is not so depressed. The value of $T_{m,PCL}$ for PCL-*b*-PE is always higher than that for PCL-*b*-PB, and the difference in $T_{m,PCL}$, ΔT_m, increases steadily with increasing ϕ_{PCL}. However, ΔT_m drops to almost zero when the PCL block in PCL-*b*-PE crystallizes in the microdomain structure without forming the PE lamellar morphology, which will be ascribed to the recovery of conformational entropy in the amorphous PCL block. The chain stretching of PCL blocks confined in the PE lamellar morphology is discussed on the basis of ΔT_m.
Polymer Journal (2011) **43,** 370–377; doi:10.1038/pj.2011.4; published online 9 February 2011

Keywords: crystalline–crystalline diblock copolymer; lamellar morphology; melting temperature

INTRODUCTION

The crystallization of crystalline–amorphous diblock copolymers yields a variety of crystallized morphologies in the system. When the microdomain structure existing in the melt is not stable against crystallization, it will be transformed into the crystallized lamellar morphology, an alternating structure consisting of lamellar crystals and amorphous layers, by the crystallization of constituent blocks (upper panel in Figure 1).[1–5] In the crystallized lamellar morphology (right part of the upper panel), the amorphous blocks are moderately stretched in the direction parallel to the lamella surface normal, the degree of which largely depends on the molecular characteristics of block copolymers and the thickness ratio of crystalline and amorphous layers. That is, the conformational entropy is depressed for such amorphous blocks as compared with equivalent blocks without any spatial confinement. This chain stretching of amorphous blocks in the crystallized lamellar morphology of crystalline–amorphous diblock copolymers is theoretically predicted[6,7] and also experimentally verified.[8–10]

The crystalline–crystalline diblock copolymers with separate melting temperatures $T_{m,1}$ and $T_{m,2}$ ($T_{m,1} \gg T_{m,2}$) behave as crystalline–amorphous diblocks at temperatures higher than $T_{m,2}$.[11–15] The lower panel in Figure 1 schematically shows the morphology formation in an asymmetric crystalline–crystalline diblock copolymer with an extremely minor higher-T_m block. When this copolymer is quenched into temperatures between $T_{m,1}$ and $T_{m,2}$, the higher-T_m blocks with $T_{m,1}$ crystallize first to form the crystallized lamellar morphology (middle part of the lower panel). Therefore, as is the case for amorphous blocks in crystalline–amorphous blocks, the amorphous lower-T_m blocks will deform within this lamellar morphology to reduce their conformational entropy. The lower-T_m blocks finally crystallize at temperatures below $T_{m,2}$ in the crystallized lamellar morphology (right part of the lower panel) with $-\Delta S_2$ (entropy decrease of lower-T_m blocks in crystalline–crystalline diblocks). In this study, ΔS_2 will be significantly smaller than ΔS_1, where $-\Delta S_1$ is the entropy decrease of crystalline blocks in crystalline–amorphous diblocks on crystallization.

In general, the melting temperature T_m of crystalline polymers is determined by a delicate balance between the change in enthalpy and entropy at T_m through the equation

Department of Organic and Polymeric Materials, Graduate School of Science and Engineering, Tokyo Institute of Technology, Tokyo, Japan
Correspondence: Dr S Nojima, Department of Organic and Polymeric Materials, Graduate School of Science and Engineering, Tokyo Institute of Technology, H-125, 2-12-1 Ookayama, Meguro-Ku, Tokyo 152-8552, Japan.
E-mail: snojima@polymer.titech.ac.jp
Received 22 October 2010; revised and accepted 7 January 2011; published online 9 February 2011

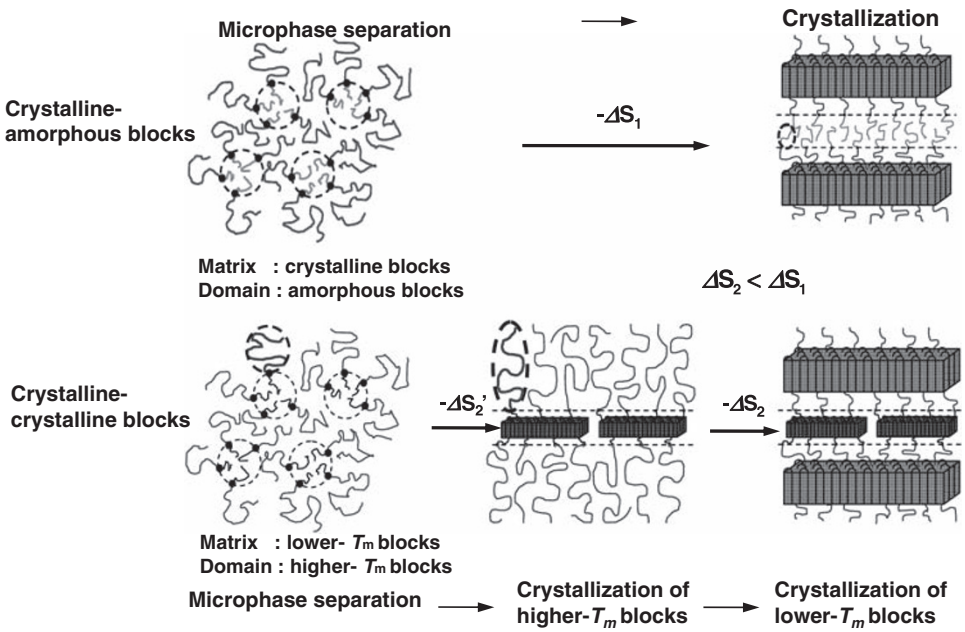

Figure 1 Schematic illustration showing the morphology formation of crystalline–amorphous diblock copolymers (upper panel) and crystalline–crystalline diblock copolymers (lower panel). In crystalline–crystalline diblocks, the higher-T_m block crystallizes first to yield the solid lamellar morphology, even if it is a minor component in the system (middle part of the lower panel), where the amorphous lower-T_m block is moderately stretched in the direction parallel to the lamella surface normal. Therefore, the entropy difference between the amorphous and crystallized states of lower-T_m blocks in crystalline–crystalline diblocks, ΔS_2, is smaller than that of crystalline blocks in crystalline–amorphous diblocks, ΔS_1.

$$T_m = \frac{\Delta H_m}{\Delta S_m} \quad (1)$$

where ΔH_m and ΔS_m are the difference in enthalpy and entropy between perfect crystals and amorphous chains at T_m, respectively. Therefore, the T_m of lower-T_m blocks in crystalline–crystalline diblocks (that is, $T_{m,2}$) will increase as compared with that of equivalent crystalline blocks in crystalline–amorphous diblocks because ΔS_m is moderately reduced (that is, $\Delta S_2 < \Delta S_1$), which originally arises from the spatial confinement of lower-T_m blocks imposed by the lamellar morphology formed by the advance crystallization of higher-T_m blocks.

In this study, we investigate the melting temperature of poly(ε-caprolactone) (PCL) blocks (lower-T_m blocks) in PCL-*block*-polyethylene (PCL-*b*-PE) diblock copolymers, for which we have recently conducted extensive studies on the crystallization behavior and final morphology.[16–21] We prepare several asymmetric PCL-*b*-PE copolymers with PE blocks (higher-T_m blocks) as a minor component, so that PCL blocks will deform in the preexisting lamellar morphology formed by the crystallization of PE blocks (PE lamellar morphology). As a result, ΔS_m of PCL blocks (that is, ΔS_2 in Figure 1) will be smaller than that in crystalline–amorphous diblocks (ΔS_1), yielding a significant increase in T_m. From the experimental results, we discuss the chain stretching of PCL blocks in the PE lamellar morphology.

EXPERIMENTAL PROCEDURE

Samples

The samples used in this study are PCL-*b*-PE diblock copolymers with the PE block as a minor component, which were obtained by the hydrogenation of PCL-*block*-polybutadinene (PCL-*b*-PB) diblock copolymers anionically synthesized. The PCL-*b*-PB synthesis and the subsequent hydrogenation of PB blocks have been described in our previous publications.[16,17,22,23] The results of molecular characterization for PCL-*b*-PE copolymers are shown in Table 1, where the numeral in the sample code represents the volume % of PCL blocks in the copolymer. The following specific volumes were used to calculate the volume fraction of each block in PCL-*b*-PE from the ^{1}H nuclear magnetic resonance data: for amorphous PE[24]

$$v_{sp}(T) = 1.1696 + (1.77 \times 10^{-4}) \times T \quad (2)$$

and for amorphous PCL,[25]

$$v_{sp}(T) = 0.9106 + (6.01 \times 10^{-4}) \times T \quad (3)$$

where $v_{sp}(T)$ is in $cm^3\,g^{-1}$ and T in °C.

Table 1 Molecular characteristics of PCL-*b*-PE used in this study

Sample code	M_n[a] Total	PCL block	PE block	M_w/M_n[b]	PCL:PE[c] (Vol. %)	$T_{m,PCL}$[d] (°C)	$T_{m,PE}$[d] (°C)
C91	10 000	9300	700	1.07	91:9	(57.5)	—
C90	40 000	37 000	3000	1.31	90:10	(61.1)	(94.1)
C86	24 000	21 000	3000	1.21	86:14	62.3	96.1
C81	19 000	16 000	3000	1.19	81:19	61.4	90.4
C74	16 000	12 000	4000	1.16	74:26	60.6	97.4
C71	14 000	11 000	3000	1.16	71:29	59.9	97.7
C64	14 000	10 000	4000	1.16	64:36	59.5	94.9
C51	18 000	10 000	8000	1.18	51:49	59.1	95.2

Abbreviations: DSC, differential scanning calorimetry; GPC, gel permeation chromatography; MO, membrane osmometry; NMR, nuclear magnetic resonance;
PCL, poly(ε-caprolactone); PCL-*b*-PE, PCL-*block*-polyethylene.
[a]Determined by MO.
[b]Determined by GPC.
[c]Determined by ^{1}H-NMR using equations (2) and (3).
[d]Determined by DSC during heating at 10 °C min^{-1}. The samples were first annealed at 70 °C for 100 min to crystallize PE blocks and then annealed at 45 °C for 100 min to crystallize PCL blocks. The melting temperature in the parenthesis indicates that the system takes the crystallized microdomain structure.

Thermal history applied to the samples

The PCL-*b*-PE copolymer was first annealed at 120 °C for ~10 min to completely erase the effect of PE and PCL crystals, and then quenched into 70 °C (lower than the crystallizable temperature of PE blocks but higher than the melting temperature of PCL blocks), at which the PE block was crystallized for 100 min to form the PE lamellar morphology. Subsequently, the copolymer was quenched again into lower crystallization temperatures T_c ranging from 10 to 50 °C, at which the PCL blocks were crystallized for 100 min within the PE lamellar morphology. The PCL-*b*-PB copolymers, which were the precursors of PCL-*b*-PE copolymers and hence had an identical PCL molecular weight, were also used to obtain the melting temperature of PCL blocks with no spatial confinement by the PE lamellar morphology. The PCL-*b*-PB copolymers were directly quenched from 120 °C into T_c to crystallize PCL blocks without annealing at 70 °C.

Differential scanning calorimetry measurements

A DSC Pyris I (Perkin Elmer Instruments LLC, Shelton, CT, USA) was used to evaluate the melting temperature and crystallinity of both blocks during heating at 10 °C min^{-1}. The temperature calibration was carried out using indium (T_m=156.6 °C) and *n*-octadecane (T_m=27.6 °C). The melting temperature of PCL blocks ($T_{m,PCL}$) and PE blocks ($T_{m,PE}$) was obtained from the peak temperature of the differential scanning calorimetry (DSC) endothermic curve. The crystallinity of PCL blocks, χ_{PCL}, was calculated from the endothermic peak area during heating by assuming that the heat of fusion for perfect PCL crystals was 135 J g^{-1}.[25]

Small-angle X-ray scattering measurements

The morphology formed at each temperature was mainly investigated using the synchrotron small-angle X-ray scattering (SAXS) method and complementarily using the conventional SAXS method. The results obtained by the two methods coincided with each other, and no systematic error could be detected.

The synchrotron SAXS measurement was taken at the Photon Factory in High Energy Acceleration Research Organization, Tsukuba Japan, with a small-angle X-ray equipment for solution installed at beam line BL-10C. Details of the equipment and instrumentation have already been described elsewhere.[9,26] The SAXS intensity was detected using an image plate system R-AXIS VII (Rigaku Co., Tokyo, Japan). The two-dimensional SAXS curves thus obtained were first converted into one-dimensional curves using a circular averaging program, and then corrected for background scattering. The SAXS curves were finally obtained as a function of wave number s (=$(2/\lambda)\sin\theta$, λ: X-ray wavelength (=0.1488 nm) and 2θ: scattering angle) to evaluate the alternating distance of the morphology formed in the system.

The conventional SAXS measurement was taken using a Nano-Viewer (Rigaku Co.) with a rotating anode X-ray generator operating at 45 kV and 60 mA. The detector was a one-dimensional position-sensitive proportional counter with an accumulation time of 1 h, and the method of data treatment was the same as that for synchrotron SAXS results.

RESULTS

Morphology before and after crystallization of PE and PCL blocks

We first crystallized PE blocks in every PCL-*b*-PE copolymer at 70 °C. It is important to confirm that the crystallization of PE blocks yields the solid lamellar morphology, an alternating structure consisting of PE lamellar crystals and amorphous PCL + PE layers (PE lamellar morphology). This is because the formation of the PE lamellar morphology is absolutely necessary to deform to a large extent the amorphous PCL blocks (middle part of lower panel in Figure 1).

Figure 2 shows the one-dimensional SAXS curves for C74 (a) and C90 (b) measured at each temperature indicated. The gray curve obtained at 110 °C represents the SAXS curve from the microdomain structure existing in the melt, whereas the black ones from the morphology after the crystallization of PE blocks (80 and 60 °C) and PE+PCL blocks (40 and 20 °C). In C74 (Figure 2-a), the SAXS curve at 110 °C has several scattering peaks, the positions of which exactly correspond to a ratio of 1:2:$\sqrt{7}$:4. This SAXS curve, together

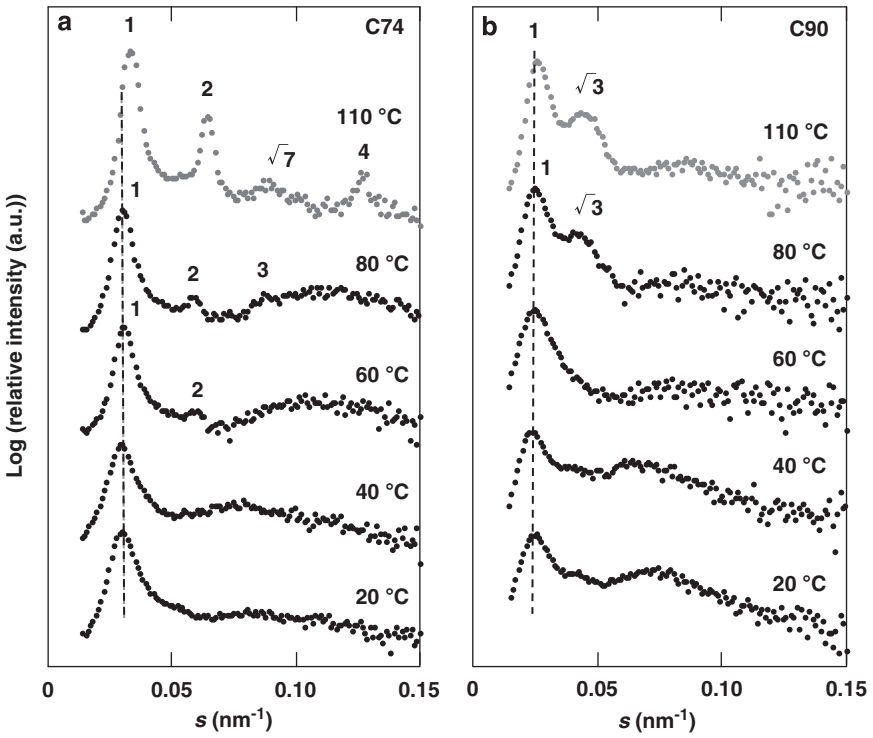

Figure 2 One-dimensional small-angle X-ray scattering curves for C74 (**a**) and C90 (**b**) measured at each temperature indicated. The gray curve arises from the molten microdomain structure and the black ones from the solid lamellar morphology (C74) or the crystallized microdomain structure (C90) after the crystallization of polyethylene (PE) or PE+poly(ε-caprolactone) blocks.

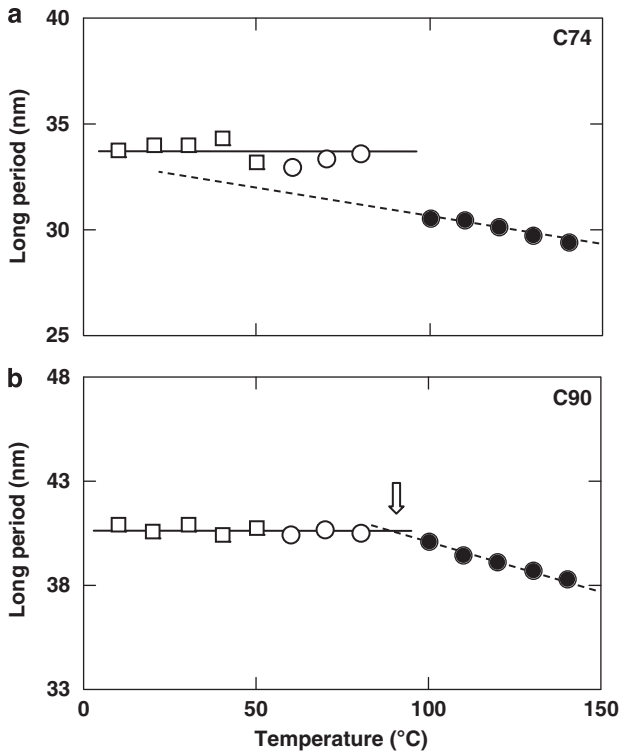

Figure 3 Long period plotted against temperature for C74 (**a**) and C90 (**b**). ●: Both polyethylene (PE) and poly(ε-caprolactone) (PCL) blocks amorphous. ○: PE blocks crystallized but PCL blocks amorphous. □: Both blocks crystallized.

with the volume fraction of PCL blocks (∼0.74), indicates that the cylindrical microdomain structure is formed in the melt. However, the shape of SAXS curves below 80 °C is significantly different from that at 110 °C with the primary peak position slightly moving to the lower angle (broken line), suggesting that morphological transition occurs by the crystallization of PE blocks (break-out crystallization). In C90 (Figure 2-b), however, the SAXS curve at 110 °C is almost similar to those below 80 °C with the primary peak position being unchanged, suggesting that the crystallization of PE and/or PCL blocks occurs within the microdomain structure existing in the melt (confined crystallization).

Figure 3 shows the long period (LP), an alternating distance of the morphology evaluated from the primary peak position of SAXS curves shown in Figure 2, plotted against temperature for C74 (a) and C90 (b), where the closed circle represents the results above the melting temperature of both blocks (⩾100 °C) and hence indicates LP for the microdomain structure. The open circle and square represent the results at lower temperatures, at which PE blocks or PE+PCL blocks crystallize in the system, respectively. LP for the molten microdomain structure increases steadily with decreasing temperature for both copolymers, which arises from several factors such as change in block incompatibility and chain conformation.[27,28] The extrapolated LP to low temperatures for C74 is significantly smaller than that for the PE (and also for PE + PCL-)-crystallized morphology, and eventually LP changes discontinuously before and after the crystallization of PE blocks at ∼95 °C. This fact clearly indicates that the morphology is transformed by the crystallization of PE blocks, and the PE lamellar morphology is finally formed in the system. This discontinuous change in LP with decreasing temperature is reported for other crystalline–amorphous diblocks[20,29] in which break-out crystallization (that is, the morphological transition from the molten microdomain structure into the crystallized lamellar morphology) is confirmed. We obtained the same results for C51–C86. Note that the constant LP of the PE-crystallized morphology below 95 °C arises from the fact that the crystallization of PE blocks is extremely fast, so that it finishes substantially during quenching into the crystallization temperature.

It is easily expected for C51–C86 that the formation of the PE lamellar morphology will affect the amorphous PCL blocks to yield the deformed PCL conformation stretching in the direction parallel to the lamella surface normal. This is because the volume fraction of PE blocks in our copolymers is smaller than that of PCL blocks; however, the copolymers should take the alternating structure of crystalline lamellae and amorphous layers after the crystallization of PE blocks, and eventually the amorphous PCL blocks are stretched, if we assume the incompressibility of amorphous PCL blocks intervening between the PE lamellar crystals (middle part of the lower panel in Figure 1).

Figure 3-b indicates that the morphology formed in C90 (and also C91) is frozen after the crystallization of PE blocks, with LP exactly corresponding to that of the microdomain structure existing just before the crystallization of PE blocks (shown by an arrow in Figure 3-b); that is, the microdomain structure is completely preserved and the PE blocks crystallize within this structure (confined crystallization). This confined crystallization is also reported for PE-containing crystalline–amorphous diblocks with a relatively low-molecular weight.[30,31] As a result, the conformation of amorphous PCL blocks does not change so much when it is compared with that in the molten microdomain structure.

In summary, the morphological transition from the microdomain structure into the PE lamellar morphology was observed for C51–C86 by the crystallization of PE blocks. However, the molten microdomain structure was completely preserved in C91 and C90 after the crystallization of PE blocks to form the crystallized microdomain structure. We can expect that the conformation of PCL blocks in the PE lamellar morphology is more stretched than that in the crystallized microdomain structure.

Morphological change by changing thermal history

We found from Figures 2 and 3 that the morphology after the crystallization of PE blocks at 70 °C was the PE lamellar morphology for C51–C86, whereas it was the crystallized microdomain structure for C90 and C91. However, we found that we could change the morphology formed in C91 and C86 by changing the thermal history applied to the sample.

We found that the morphology of C91 after the crystallization of PE blocks changed from the microdomain structure into the PE lamellar morphology by annealing it at 80 °C for a very long time (∼3 days). Figure 4-a shows the one-dimensional SAXS curves of C91 obtained at each temperature indicated, where the SAXS curve at 80 °C was measured after the thermal treatment described above. The primary peak position at 70 °C is almost the same as that at 110 °C, indicating that the PE block crystallizes within the microdomain structure, as is the case for C90 (Figure 2-b). However, we obtained the different SAXS curve with the primary peak position moving fairly to the lower angle when C91 was annealed at 80 °C for 3 days, suggesting that the microdomain structure was slowly transformed into the PE lamellar morphology by the crystallization of PE blocks at 80 °C. That is, the slight difference in crystallization temperature yielded the completely different morphology in C91; the crystallized microdomain structure prevailed in the system at 70 °C owing mainly to the rapid crystallization of PE blocks, whereas slow crystallization of PE blocks at 80 °C destroyed the molten microdomain structure to form the PE lamellar morphology. However, this morphological transition could not be

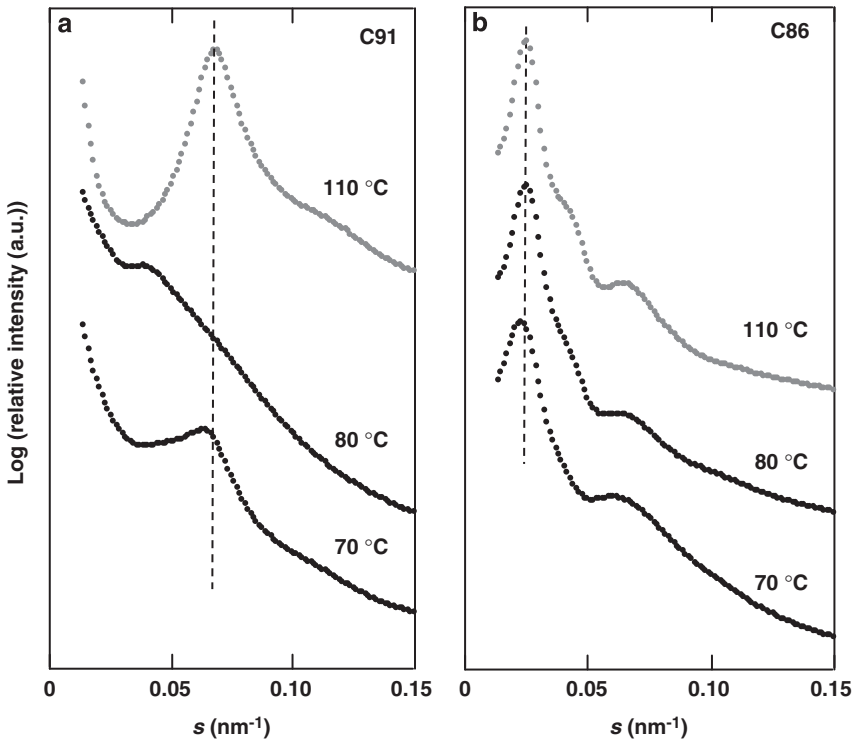

Figure 4 One-dimensional small-angle X-ray scattering (SAXS) curves for C91 (**a**) and C86 (**b**) measured at each temperature indicated. The SAXS curve for C91 measured at 80 °C was obtained by annealing it at 80 °C for 3 days. The SAXS curve for C86 at 80 °C was obtained by quenching it into liquid nitrogen to fix the microdomain structure, followed by gradual temperature increase up to 80 °C.

observed in C90, probably because of the fact that the total molecular weight of C90 was considerably higher than that of C91 (Table 1).

We quenched C86 into liquid nitrogen to fix the microdomain structure and after that, the temperature was gradually increased up to 80 °C. Both PE and PCL blocks crystallized during temperature increase to yield the crystallized microdomain structure instead of the PE lamellar morphology formed at 70 °C, which was confirmed by the unchanged peak position in the SAXS curves at 110 and 80 °C (Figure 4-b). That is, LP is 40.6 nm at 110 and 80 °C, whereas it is 44.9 nm at 70 °C. However, C51–C81 could not give the crystallized microdomain structure even when this quenching method was used, for which the increasing driving force for PE crystallization will be responsible. Two different morphologies formed in C91 and C86 after the crystallization of PE blocks are expected to yield the difference in the melting behavior of PCL blocks, as we will present later.

In summary, we could obtain two different morphologies, the PE lamellar morphology and crystallized microdomain structure, only for C91 and C86 after the crystallization of PE blocks. That is, the crystallized microdomain structure was formed by the crystallization of C91 at 70 °C, whereas annealing C91 at slightly higher temperature (~80 °C) for an extremely long time (~3 days) yielded the PE lamellar morphology. When C86 was quenched into liquid nitrogen, the microdomain structure was preserved to form the crystallized microdomain structure after gradual increase in temperature, whereas the PE lamellar morphology prevailed in the system after direct crystallization of C86 at 70 °C.

Melting behavior of PCL blocks

The melting behavior of PCL blocks in PCL-*b*-PE and PCL-*b*-PB was investigated using DSC with a heating rate of 10 °C min^{-1}. Figure 5-a shows the typical DSC curves for C74 and B74 (the precursor of C74), first kept at 70 °C for 100 min to crystallize PE blocks and then annealed at 45 °C for 100 min to crystallize PCL blocks. We find a sharp endothermic peak at ~60 °C arising from the melting of PCL blocks. In addition, an extremely diffused endothermic peak can be observed at ~97 °C in the DSC curve of C74 (indicated by an arrow). From these DSC curves, we evaluated the melting temperature of PCL blocks, $T_{m,PCL}$, and of PE blocks, $T_{m,PE}$, in PCL-*b*-PE (shown in Table 1) and $T_{m,PCL}$ in PCL-*b*-PB. We observe from Table 1 that $T_{m,PCL}$ decreases steadily with a decrease in the volume fraction of PCL blocks in the system, ϕ_{PCL}. The melting temperature of crystalline chains is, in general, closely dependent on their molecular weight, as well as on the crystallization temperature and other factors,[32] so that we cannot find out the true reason for the change in $T_{m,PCL}$ shown in Table 1. Therefore, we evaluated the melting temperature difference ΔT_m between PCL blocks in PCL-*b*-PE and those in PCL-*b*-PB (the precursor of PCL-*b*-PE with an identical PCL molecular weight) to exclude the effect of PCL molecular weight on $T_{m,PCL}$. The ϕ_{PCL} dependence of ΔT_m will give important information when we discuss the melting behavior difference between PCL blocks with different conformations after melting.

Figure 5-b shows ΔT_m plotted against ϕ_{PCL}, where the open circle represents the results for PCL-*b*-PE with the PE lamellar morphology and the closed circle represents those for PCL-*b*-PE with the crystallized microdomain structure. We observe from Figure 5-b that ΔT_m for the PE lamellar morphology increases steadily with increasing ϕ_{PCL}. That is, ΔT_m increases from 0.5 to 3.4 °C between ϕ_{PCL}=0.51 and 0.91, and it does not depend on T_c, although $T_{m,PCL}$ increases moderately with increasing T_c (for example, $T_{m,PCL}$=58.7 °C at T_c=36 °C and $T_{m,PCL}$=60.6 °C at T_c=45 °C for ϕ_{PCL}=0.74).

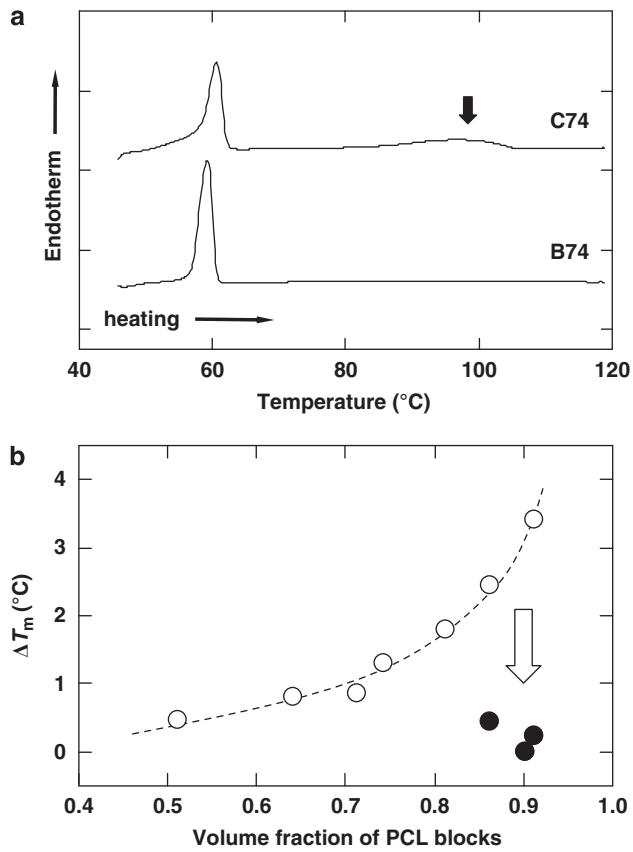

Figure 5 (**a**) Differential scanning calorimetry curves for C74 and B74 (the precursor of C74) during heating at 10 °C min^{-1}. The endothermic peak appearing at ~60 °C arises from the melting of poly(ε-caprolactone) (PCL) blocks and that at ~97 °C (indicated by an arrow) from the melting of polyethylene (PE) blocks. (**b**) The difference in melting temperature ΔT_m between PCL blocks in PCL-*block*-PE and in PCL-*block*-polybutadiene plotted against ϕ_{PCL}. ○: The PE lamellar morphology is formed by the crystallization of PE blocks (break-out crystallization). ●: The microdomain structure is preserved after the crystallization of PE blocks (confined crystallization).

In addition, we can observe that ΔT_m for the crystallized microdomain structure is very small, although it takes a large ΔT_m for the PE lamellar morphology. For example, ΔT_m is 0.3 °C for the crystallized microdomain structure of C91 and ΔT_m is 3.4 °C for the PE lamellar morphology. This difference in ΔT_m will arise mainly from the difference in conformation of amorphous PCL blocks, which originates from the difference in morphology after the crystallization of PE blocks. We will discuss the conformation of amorphous PCL blocks in the PE lamellar morphology as a function of ϕ_{PCL} by evaluating the degree of chain stretching for PCL blocks in the next section.

In summary, the DSC results showed that the melting temperature difference ΔT_m was significantly large between PCL blocks in PCL-*b*-PE with the PE lamellar morphology and those in PCL-*b*-PB (the precursor of PCL-*b*-PE with an identical PCL molecular weight), and ΔT_m increased steadily with increasing ϕ_{PCL}. In addition, we found a considerable difference in ΔT_m between PCL blocks in the crystallized microdomain structure and those in the PE lamellar morphology for the limited copolymers (that is, C86 and C91). This difference in ΔT_m will arise from the difference in the chain conformation between amorphous PCL blocks existing in two morphologies.

DISCUSSION

Chain stretching of amorphous PCL blocks in the PE lamellar morphology

In this study, we try to evaluate the degree of chain stretching of amorphous PCL blocks confined in the PE lamellar morphology from the ϕ_{PCL} dependence of ΔT_m shown in Figure 5-b. In general, the melting temperature is expressed using the change in enthalpy, ΔH_m, and entropy, ΔS_m, at the melting point (equation (1)),[33] so that ΔT_m can be represented as

$$\Delta T_m = T_{m,2} - T_{m,1} = \frac{\Delta H_m}{\Delta S_{2,m}} - \frac{\Delta H_m}{\Delta S_{1,m}} \quad (4)$$

where $T_{m,1}$ is the melting temperature of PCL blocks in PCL-*b*-PB and $T_{m,2}$ is that in PCL-*b*-PE, and $\Delta S_{1,m}$ and $\Delta S_{2,m}$ are the changes in conformational entropy of PCL blocks in PCL-*b*-PB and PCL-*b*-PE, respectively, due to the melting. ΔH_m is the change in enthalpy by melting for PCL blocks and will be the same for both systems. Therefore, equation 4 can be rewritten as

$$\Delta T_m = \frac{\Delta H_m \delta S}{\Delta S_{1,m} \Delta S_{2,m}} \quad (5)$$

where $\delta S = \Delta S_{1,m} - \Delta S_{2,m}$ and represents the difference in conformational entropy between amorphous PCL blocks in PCL-*b*-PB and those in PCL-*b*-PE. If we assume that δS is sufficiently small when compared with $\Delta S_{1,m}$ and $\Delta S_{2,m}$ (that is, $\Delta S_{1,m} \sim \Delta S_{2,m}$), and that ΔH_m and $\Delta S_{1,m}$ are approximated by their equilibrium values ΔH_m° and ΔS_m° of PCL chains because the PCL blocks in PCL-*b*-PB are not so deformed, we have

$$\Delta T_m \sim \frac{\Delta H_m^o}{(\Delta S_m^o)^2} \delta S \quad (6)$$

The change in conformational entropy δS due to chain stretching is related to the degree of chain stretching λ for one PCL block through the equation[34–36]

$$\delta S = \frac{k}{2(M_n/N_A)} \left(\lambda^2 + \frac{2}{\lambda} - 3 \right) \quad (7)$$

where k is the Boltzmann constant, N_A the Avogadro's constant and M_n the molecular weight of PCL blocks (Table 1). From the equilibrium melting temperature T_m° (=342 K)[37] and the heat of fusion for perfect PCL crystals ΔH_m° (=135 J g^{-1}),[25] we find λ from ΔT_m throughequations (6) and (7).

Figure 6 shows δS for 1 g PCL blocks and λ for one PCL block plotted against ϕ_{PCL}, where δS increases steadily with increasing ϕ_{PCL}, suggesting that the conformational entropy of PCL blocks confined in the PE lamellar morphology is considerably reduced when it is compared with that in PCL-*b*-PB. That is, PCL-*b*-PB forms the microdomain structure after melting of PCL blocks, so that they are not so deformed, whereas PCL-*b*-PE takes the PE lamellar morphology and the PCL blocks are significantly deformed (middle part of the lower panel in Figure 1). The degree of chain stretching λ for one PCL block also increases with increasing ϕ_{PCL}, as shown in Figure 6. However, λ for C91 is moderately small, which is ascribed to the low-molecular weight of PCL blocks. That is, δS represents the entropy change per 1 g of PCL blocks, whereas λ represents the degree of stretching for one PCL block.

In summary, we find from the ΔT_m values observed in Figure 5-b that the amorphous PCL blocks in the PE lamellar morphology of PCL-*b*-PE are significantly stretched when compared with those in the molten microdomain structure in PCL-*b*-PB, and the degree of chain stretching increases steadily with increasing ϕ_{PCL}. The asymmetry of layer thickness between crystallized PE layers and amorphous PCL

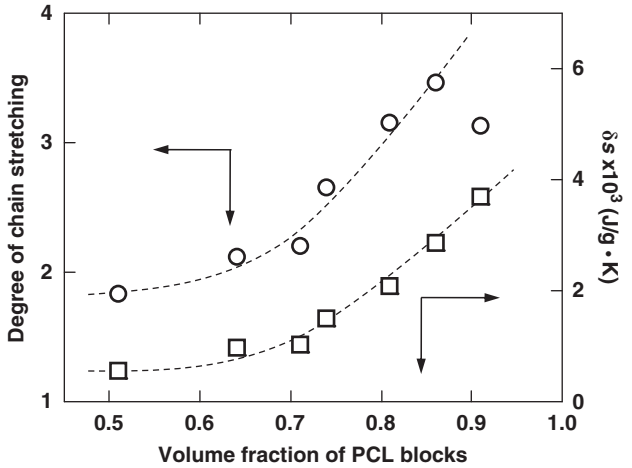

Figure 6 Entropy difference δS between poly(ε-caprolactone) (PCL) blocks in PCL-*block*-polyethylene (PCL-*b*-PE) and in PCL-*block*-polybutadiene (□), and the degree of chain stretching for one PCL block in PCL-*b*-PE (○) plotted against ϕ_{PCL}.

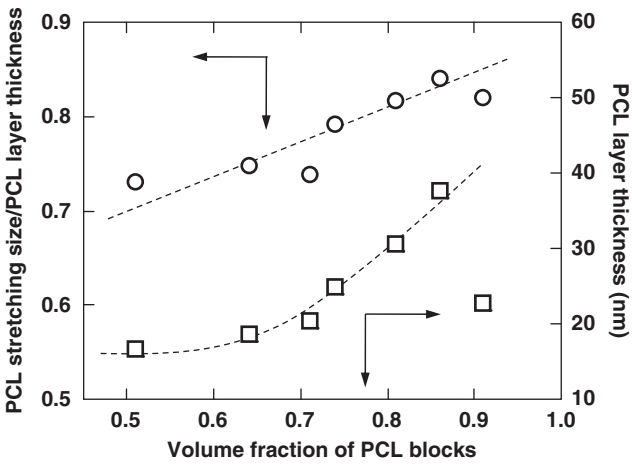

Figure 7 Thickness of poly(ε-caprolactone) (PCL) layers in the polyethylene lamellar morphology (□) and PCL stretching size/PCL layer thickness (○) plotted against ϕ_{PCL}.

layers in the PE lamellar morphology is responsible for the extreme chain stretching of amorphous PCL blocks.

Relationship between stretched PCL size and PCL layer thickness

We quantitatively consider the relationship between the stretched size of amorphous PCL blocks and the total thickness of PCL layers in the PE lamellar morphology. Figure 7 shows the thickness of PCL layers in the PE lamellar morphology plotted against ϕ_{PCL}, which was evaluated from ϕ_{PCL} (Table 1) and LP obtained by SAXS results (Figure 2) by considering the crystallinity of PE blocks. The thickness of PCL blocks increases steadily with increasing ϕ_{PCL} except for C91. The PCL layer thickness for C91 is considerably small, which may arise from the extremely small-molecular weight of PCL blocks in C91 ($\sim$700).

To intuitively understand the relationship between the stretched PCL size d and PCL layer thickness, we evaluated the ratio of these two values, where d was calculated[8] from $d=2\langle S^2\rangle^{1/2}=(2a/\sqrt{6})M_n^{1/2}$ ($\langle S^2\rangle$: mean-square radius of gyration) with a=0.0799 nm.[38] The result is also shown in Figure 7. We find that one PCL block occupies 72–82% of the PCL layer thickness in the PE lamellar morphology depending on ϕ_{PCL}. For the crystallized lamellar morphology formed in crystalline–amorphous diblock copolymers, we usually assume two limited models to predict the molecular weight and composition dependence of the morphology; single-layer model and double-layer model, where the former means that one crystalline block occupies the whole layer and the latter that one crystalline block occupies the half thickness of the total layer. Our result shown in Figure 7 is just intermediate between two models, and the ratio of the stretched PCL size and PCL layer thickness depends slightly on ϕ_{PCL}. This result suggests that one PCL block takes heterogeneous conformation in the PCL layer; that is, the PCL chain is slightly dense near the junction point and sparse at the free chain end to avoid the excess overlap between adjacent blocks at the middle of PCL layers.

In summary, one stretched PCL block in PCL-*b*-PE occupied 72–82% of the total PCL layer thickness in the PE lamellar morphology. This result is intermediate between the single- and double-layer models usually used to predict the molecular weight dependence of the crystallized lamellar morphology formed in crystalline–amorphous diblock copolymers.

CONCLUSIONS

The melting temperature of PCL blocks, spatially confined in the solid lamellar morphology formed by the crystallization of PE blocks in PCL-*b*-PE copolymers, was investigated using DSC as a function of the volume fraction of PCL blocks in the system, ϕ_{PCL}. The morphology in the melt and crystallized state was also investigated using small-angle X-ray scattering (SAXS). The melting temperature difference between PCL blocks in PCL-*b*-PE and PCL-*block*-polybutadiene (PCL-*b*-PB), the precursor of PCL-*b*-PE with an identical PCL molecular weight, was evaluated as a function of ϕ_{PCL}, and discussed on the basis of the crystallized morphology formed in the system. The following conclusions were obtained from this study.

The crystallization of PE blocks yielded the morphological transition from the microdomain structure into the crystallized lamellar morphology, except for two samples with large ϕ_{PCL} (C90 and C91), in which the microdomain structure was preserved after the crystallization of PE blocks.

The melting temperature of PCL blocks, $T_{m,PCL}$, in PCL-*b*-PE with the crystallized lamellar morphology was always higher than that in corresponding PCL-*b*-PB, and the difference in $T_{m,PCL}$, ΔT_m, increased steadily with increasing ϕ_{PCL}.

The value of ΔT_m decreased drastically when PCL blocks were crystallized in the microdomain structure. These results could be successfully explained by considering the difference in chain stretching between PCL blocks confined in the crystallized lamellar morphology and those in the microdomain structure.

ACKNOWLEDGEMENTS

The 1D-SAXS measurement has been performed under the approval of the Photon Factory Advisory Committee (No. 2010G014).

1 Hamley, I. W. *The Physics of Block Copolymers* (Oxford University Press, Oxford, 1998).
2 Loo, Y. L. & Register, R. A. *Developments in Block Copolymer Science and Technology* (ed. Hamley, I.W.) Ch. 6, 213–243 (Wiley, New York, 2004).
3 Muller, A. J., Balsamo, V. & Arnal, M. L. Nucleation and crystallization in diblock and triblock copolymers. *Adv. Polym. Sci.* **190,** 1–63 (2005).
4 Nandan, B., Hsu, J. Y. & Chen, H. L. Crystallization behavior of crystalline-amorphous diblock copolymers consisting of a rubbery amorphous block. *J. Macromol. Sci.* **46,** 143–172 (2006).

5 Castillo, R. V. & Muller, A. J. Crystallization and morphology of biodegradable or biostable single and double crystalline block copolymers. *Prog. Polym. Sci.* **34,** 516–560 (2009).
6 DiMarzio, E. A., Guttman, C. M. & Hoffman, J. D. Calculation of lamellar thickness in a diblock copolymer, one of whose components is crystalline. *Macromolecules* **13,** 1194–1198 (1980).
7 Whitmore, M. D. & Noolandi, J. Theory of crystallizable block copolymer blends. *Macromolecules* **21,** 1482–1496 (1988).
8 Nojima, S., Yamamoto, S. & Ashida, T. Crystallization of block copolymers IV. Molecular weight dependence of the morphology formed in ε-caprolactone-butadiene diblock copolymers. *Polym. J.* **27,** 673–682 (1995).
9 Nojima, S., Kikuchi, N., Rohadi, A., Tanimoto, S. & Sasaki, S. Melting behavior of poly(ε-caprolactone)-*block*-polybutadiene copolymers. *Macromolecules* **32,** 3727–3734 (1999).
10 Lee, L. W. & Register, R. A. Equilibrium control of crystal thickness and melting point through block copolymerization. *Macromolecules* **37,** 7278–7284 (2004).
11 Hillmyer, M. A. & Bates, F. S. Influence of crystallinity on the morphology of poly(ethylene oxide) containing diblock copolymers. *Macromol. Symp.* **117,** 121–130 (1997).
12 Sun, L., Liu, Y., Zhu, L., Hsiao, B. S. & Avila-Orta, C. A. Self-assembly and crystallization behavior of a double-crystalline polyethylene-*block*-poly(ethylene oxide) diblock copolymer. *Polymer* **45,** 8181–8193 (2004).
13 Muller, A. J., Albuerne, J., Marquez, L., Raquez, J. M., Degee, P., Dubois, P., Hobbs, J. & Hamley, I. W. Self-nucleation and crystallization kinetics of double crystalline poly(*p*-dioxanone)-*b*-poly(ε-caprolactone) diblock copolymers. *Faraday Discuss.* **128,** 231–252 (2005).
14 Muller, A. J., Lorenzo, A. T., Castillo, R. V., Arnal, M. L., Fierro, A. B. & Abetz, V. Crystallization kinetics of homogeneous and melt segregated PE containing diblock copolymers. *Macromol. Symp.* **245,** 154–160 (2006).
15 Guo, Q., Thomann, R. & Gronski, W. Synthesis and fractionated crystallization of organic-inorganic hybrid composite materials from an amphiphilic polyethylene-*block*-poly(ethylene oxide) diblock copolymer. *Polymer* **48,** 3925–3929 (2007).
16 Nojima, S., Akutsu, Y., Washino, A. & Tanimoto, S. Morphology of melt-quenched poly(ε-caprolactone)-*block*-polyethylene copolymers. *Polymer* **45,** 7317–7324 (2004).
17 Nojima, S., Akutsu, Y., Akaba, M. & Tanimoto, S. Crystallization behavior of poly(ε-caprolactone) blocks starting from polyethylene lamellar morphology in poly(ε-caprolactone)-*block*-polyethylene copolymers. *Polymer* **46,** 4060–4067 (2005).
18 Nojima, S., Kiji, T. & Ohguma, Y. Characteristic melting behavior of double crystalline poly(ε-caprolactone)-*block*-polyethylene copolymers. *Macromolecules* **40,** 7566–7572 (2007).
19 Nojima, S., Ito, K. & Ikeda, H. Composition dependence of crystallized lamellar morphology formed in crystalline-crystalline diblock copolymers. *Polymer* **48,** 3607–3611 (2007).
20 Ikeda, H., Ohguma, Y. & Nojima, S. Composition dependence of crystallization behavior observed in crystalline-crystalline diblock copolymers. *Polym. J.* **40,** 241–248 (2008).
21 Sakurai, T., Ohguma, Y. & Nojima, S. Morphological evolution during isothermal crystallization observed in a crystalline-crystalline diblock copolymer. *Polym. J.* **40,** 971–978 (2008).
22 Nojima, S., Kato, K., Yamamoto, S. & Ashida, T. Crystallization of block copolymers. 1. Small-angle X-ray scattering study of an ε-caprolactone-butadiene diblock copolymer. *Macromolecules* **25,** 2237–2242 (1992).
23 Nojima, S., Hashizume, K., Rohadi, A. & Sasaki, S. Crystallization of ε-caprolactone blocks within a crosslinked microdomain structure of poly(ε-caprolactone)-*block*-polybutadiene. *Polymer* **38,** 2711–2718 (1997).
24 Brandrup, J. & Immergut, E. H. *Polymer Handbook* 3rd edn, (Wiley, New York, 1989).
25 Crescenzi, V., Manzini, G., Calzolari, G. & Borri, C. Thermodynamics of fusion of poly-β-propiolactone and poly-ε-caprolactone. Comparative analysis of the melting of aliphatic polylactone and polyester chains. *Eur. Polym. J.* **8,** 449–463 (1972).
26 Nojima, S., Tsutsui, H., Urushihara, M., Kosaka, W., Kato, N. & Ashida, T. A dynamic study of crystallization of poly(ε-caprolactone) and poly(ε-caprolactone)/poly(vinyl chloride) blend. *Polym. J.* **18,** 451–461 (1986).
27 Sakamoto, N. & Hashimoto, T. Order-disorder transition of low molecular weight polystyrene-*block*-polyisoprene. 1. SAXS analysis of two characteristic temperatures. *Macromolecules* **28,** 6825–6834 (1995).
28 Sakamoto, N. & Hashimoto, T. Ordering dynamics of a symmetric polystyrene-*block*-polyisoprene. 1. Ordering mechanism from the disordered state. *Macromolecules* **31,** 3292–3302 (1998).
29 Quiram, D. J., Register, R. A. & Marchand, G. R. Crystallization of asymmetric diblock copolymers from microphase-separated melts. *Macromolecules* **30,** 4551–4558 (1997).
30 Hillmyer, M. A. & Bates, F. S. Synthesis and characterization of model polyalkane-poly(ethylene oxide) block copolymers. *Macromolecules* **29,** 6994–7002 (1996).
31 Loo, Y. L., Register, R. A. & Ryan, A. J. Modes of crystallization in block copolymer microdomains: breakout, templated, and confined. *Macromolecules* **35,** 2365–2374 (2002).
32 Wunderlich, B. *Macromolecular Physics*. Vol. 3 *Crystal melting* (Academic Press, New York, 1980).
33 Mandelkern, L. *Crystallization of Polymers* (McGraw-Hill Inc., New York, 1964).
34 Kobayashi, K. & Nagasawa, T. Crystallization of sheared polymer melts. *J. Macromol. Sci.* **B4,** 331–345 (1970).
35 Peterlin, A. Crystallization from a strained melt or solution. *Polym. Eng. Sci.* **16,** 126–137 (1976).
36 Ishizuka, O. & Koyama, K. Crystallization of running filament in melt spinning of polypropylene. *Polymer* **18,** 913–918 (1977).
37 Phillips, P. J., Rensch, G. J. & Tayler, K. D. Crystallization studies of poly(ε-caprolactone). I. Morphology and kinetics. *J. Polym. Sci.* **B25,** 1725–1740 (1987).
38 Xi, X., Jiang, L., Ling, J., Sun, W. & Shen, Z. Synthesis of star-shaped poly(ε-caprolactone) by samarium-based tetrafunctional initiator and its dilute solution properties. *J. Appl. Polym. Sci.* **102,** 175–182 (2006).